Band structure effects in surface second harmonic generation: The case of Cu(001)

F. Bisio,[1,2,*] A. Winkelmann,[3] W.-C. Lin,[3,4] C.-T. Chiang,[3] M. Nývlt,[5] H. Petek,[6] and J. Kirschner[3]
[1]*CNISM, Sede Consorziata di Genova and Dipartimento di Fisica, Università di Genova, via Dodecaneso 33, I-16146 Genova, Italy*
[2]*CNR-INFM LAMIA, Corso Perrone 24, I-16152 Genova, Italy*
[3]*Max-Planck-Institut für Mikrostrukturphysik, Weinberg 2, D-06120 Halle (Saale), Germany*
[4]*Department of Physics, National Taiwan Normal University, 88, Section 4, Ting-Chou Road, Taipei 116, Taiwan*
[5]*Faculty of Mathematics and Physics, Institute of Physics, Charles University, Ke Karlovu 5, 12116 Praha 2, Czech Republic*
[6]*Department of Physics and Astronomy, University of Pittsburgh, Pittsburgh, Pennsylvania 15260, USA*
(Received 29 June 2009; revised manuscript received 31 August 2009; published 30 September 2009)

We have performed a study of simultaneous nonlinear optical second harmonic generation (SHG) and angle-resolved nonlinear photoemission at the Cu(001) surface excited by fundamental photon energies near 3 eV. At these excitation energies, we identify a dominant contribution to the SHG signal that is determined by a two-photon resonance between the *d* bands and the $n=1$ image-potential state at the Cu(001) surface. The near-resonant behavior of SHG and nonlinear photoemission is studied via Cs adsorption, which allows to systematically lower the work function and thus the reference vacuum level of the image potential. Comparison of the angle-resolved photoemission signal, arising from a restricted region of electronic momentum space, with the simultaneous optical SHG signal allows to identify an additional contribution of electronic states with nonzero surface-parallel momentum to the SHG signal enhancements. A simple model accounting for the observed behavior is developed and the implications for the quantitative understanding of SHG are discussed.

DOI: 10.1103/PhysRevB.80.125432 PACS number(s): 73.20.−r, 79.60.−i, 78.68.+m

I. INTRODUCTION

In the nonlinear optical process of second harmonic generation (SHG), optical radiation of frequency ω is coherently converted to radiation at the double frequency 2ω due to the nonlinear response of the electronic subsystem of a material.[1–3] In centrosymmetric media and under the electric dipole (ED) approximation, SHG is restricted to the symmetry-breaking surface region.[4–6] Due to its surface sensitivity, SHG has been broadly exploited to address a great variety of topics in the fields of surface and interface science, ranging from surface chemistry[7,8] to magnetism in low-dimensional systems.[9,10]

The all-optical character of SHG makes the technique applicable to insulators,[11,12] semiconductors,[13] and metals.[14] The employment of a purely optical probe allows to address solid-solid,[15] liquid-solid,[16] and air-solid[17] interfaces without encountering the experimental limitations of electron-based methods. Relying on optically induced transitions between electronic states or bands of the investigated medium, SHG is naturally sensitive to the electronic structure of the materials, with enhanced sensitivity to the surface region.[18] This great potential in terms of applicability and sensitivity is however limited by several factors, that can strongly reduce the information yield. Intrinsic to the optical probing of solid-state systems is the lack of selectivity with respect to electron crystal momentum in the SHG process.[19] This appears in strong contrast to photoemission experiments, where the dispersion of electronic states as a function of their crystal momentum *k* is directly accessed by angle-resolved electron detection.[20] Consequently, the interpretation of SHG spectra in solids has to simultaneously take into account all excitations in the whole surface Brillouin zone (BZ), where the eventual presence of strongly dispersing electronic states typically tends to wash out any potentially sharp spectral features. Independent information about the occupied and unoccupied electronic structure of the material and the extent to which resonances dominate the process has therefore to be available before the SHG yield from a given material can be correctly ascribed to specific electronic transitions,[21–23] thereby strongly limiting the predictive character of this technique. Moreover, beyond the ground-state band structure and *k*-resolved transition matrix elements, factors such as excited-state lifetimes, electronic dephasing, and collective electronic excitations (plasmons) can strongly affect SHG[24] and need to be known.

In this paper, we report a combined study of SHG and angle-resolved nonlinear photoemission of the Cu(001) surface as a function of the exposure to Cs atoms, performed with fundamental exciting photon energy in the 3 eV range. The SHG and the photoemission were excited by the same laser and were simultaneously recorded. The deposition of Cs provided a mechanism for modifying the surface electronic structure, primarily by shifting the energy position of the surface states of image-potential origin. Angle-resolved two-photon photoemission and three-photon photoemission (2PPE and 3PPE) provided momentum-resolved ($k_{\parallel}$) information about the electronic structure of the surface in the energy range probed by the SHG signal, allowing to *directly* assess the contribution of the various optically induced transitions in the material. Monitoring the SHG and 3PPE signals as a function of Cs coverage, we observed enhanced photon and electron yields in correspondence with the optically induced resonant transitions between bulk and surface electronic states. A characteristic change in the maximum of the resonant SHG yield as a function of the Cs coverage with respect to the corresponding 3PPE signal measured at $k_{\parallel}=0$ is modeled in terms of the contribution to SHG from electronic transitions with nonzero $k_{\parallel}$. A simple model for this behavior is developed, providing qualitative agreement with the experimental data.

II. EXPERIMENT

A. Apparatus

The experiments were carried out in an ultrahigh vacuum (UHV) system with a base pressure of approximately 5×10^{-11} mbar. Ultrashort excitation pulses with central energy tuneable in the range of $\hbar\omega=2.99-3.14$ eV were provided by the frequency-doubled output of a self-built Ti:sapphire oscillator. The pulse central energy could be continuously varied by tuning the phase-matching angle of the frequency-doubling 80-μm-thick β-BaB_2O_4 crystal. At the energy of $\hbar\omega=3.07$ eV, the excitation bandwidth was ~0.17 eV, the pulse length at the surface was ≤20 fs, and the pulse energy was ~1 nJ. The laser beam was focused onto the surface at an angle of incidence of 42°. The 2PPE and 3PPE spectra were measured in the normal-emission geometry, with a $k_{\|}$ resolution below ±0.07 Å^{-1}. The Cu crystal was biased at -3 V to increase the collection efficiency of electrons. The ω and 2ω components of the reflected beam exited the UHV chamber via a CaF_2 optical viewport, and were then spatially separated exploiting the optical dispersion properties of CaF_2 Brewster's angle prisms. In detail, a chain of four such prisms intercalated by adjustable slits allowed to effectively remove any spurious fundamental contribution while mantaining the spectral integrity of a sizeable SHG signal; the detected $2\omega/\omega$ intensity ratio at the detector (Perkin Elmer C922 channel photomultiplier with a CsTe solar-blind photocathode) was better than 10^4. Linear input polarization could be set to either s_{in} or p_{in} by means of an achromatic half-wave plate placed before the UHV chamber whereas the polarization of the outgoing SHG could be analyzed by means of a MgF_2 Rochon prism. The Cu(001) surface was prepared by standard sputtering and annealing procedures. The optical plane was aligned parallel to the [110] crystallographic direction. Cs was deposited from a commercial getter source. The geometrical arrangement of the apparatus allowed the simultaneous measurement of high-order photoemission in the normal-emission geometry and of SHG. The Cs-coverage dependence of both the SHG and the photoemission curves reported in this paper were measured in real time and simultaneously during the course of Cs evaporations. The background pressure during Cs deposition was lower than 5×10^{-10} mbar. All the experiments were carried out with the sample at 300 K.

B. Nonlinear photoemission spectra

In presenting the experimental data, we chose to start from the multiphoton photoemission spectra since they provide information on the optically coupled occupied/unoccupied electronic states of the sample that are prerequisite for discussing SHG. In Fig. 1, we report two multiphoton spectra measured with *p*-polarized 3.14 eV photons under normal-emission geometry for a clean Cu(001) surface (gray symbols) and after deposition of ≈0.06 monolayer of Cs [where 1 monolayer corresponds to the (2×2)Cs/Cu(001) structure, black symbols].[25–27] The energy scale is referred to the Fermi level E_F. The changes observed in the spectra upon Cs deposition reflect the corresponding variations in the interface electronic structure of the sample. The two-photon

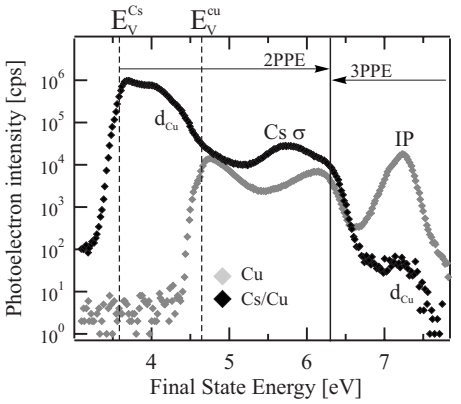

FIG. 1. Multiphoton spectra of the Cu(001) surface, before (gray symbols) and after (black symbols) the deposition of 0.1 monolayer of Cs. The spectra were measured under normal-emission geometry, with 3.14 eV photon energy.

part of the spectra, both clean and cesiated, has been discussed in depth in the literature[26,28,29] and our spectra agree with the reported data. In detail, we clearly observe the Cs-induced lowering of the work function, that allows the observation, in 2PPE, of the otherwise inaccessible Cu *d* bands (d_{Cu}) around 4 eV energy above E_F, and the appearance of a Cs adsorbate σ resonance state at a final-state energy of ~5.7 eV. The 3PPE part of the spectrum also markedly changes after the Cs deposition. In the clean Cu(001) case, the 3PPE energy range is dominated by an intense peak, ascribed to a near-resonant three-photon transition involving the Cu *d* bands as initial states, and the unoccupied Cu *sp* band (sp_{Cu}) and the $n=1$ image-potential state (IP) as intermediate states.[30] This peak, which for the the clean surface at our laser fluence accounts for more than 95% of the total 3PPE yield in the normal-emission geometry, almost completely disappears after cesiation, leaving only a shoulder in the spectrum. This behavior can be readily interpreted keeping in mind that the IP states mantain, in a first approximation, a constant binding energy with respect to the vacuum energy E_V (Ref. 31) and get broadened upon absorption of alkali atoms.[32] Thus, the work-function shift due to Cs detunes the IP state from the resonance condition and broadens it, lowering the corresponding 3PPE yield; the shoulder in the cesiated spectrum accordingly represents the three-photon replica of the large d_{Cu} peak observed in 2PPE at the low-energy end of the spectrum.

C. Second harmonic generation

The Cs-coverage dependence of the SHG yield has been measured for four different combinations of input/output $\omega/2\omega$ polarization, namely, p_{in}-p_{out}, s_{in}-p_{out}, p_{in}-s_{out}, and s_{in}-s_{out}. A sizeable SHG signal could be measured in the former two polarization combinations whereas negligible counts were recorded for p_{in}-s_{out} and s_{in}-s_{out} geometries irrespective of the Cs coverage, in agreement with expectations for electric dipole SHG from (001) surfaces and with previous experiments on the system.[33–35] In general, the p_{in}-p_{out} SHG signal is larger by roughly a factor 5–6 with respect to

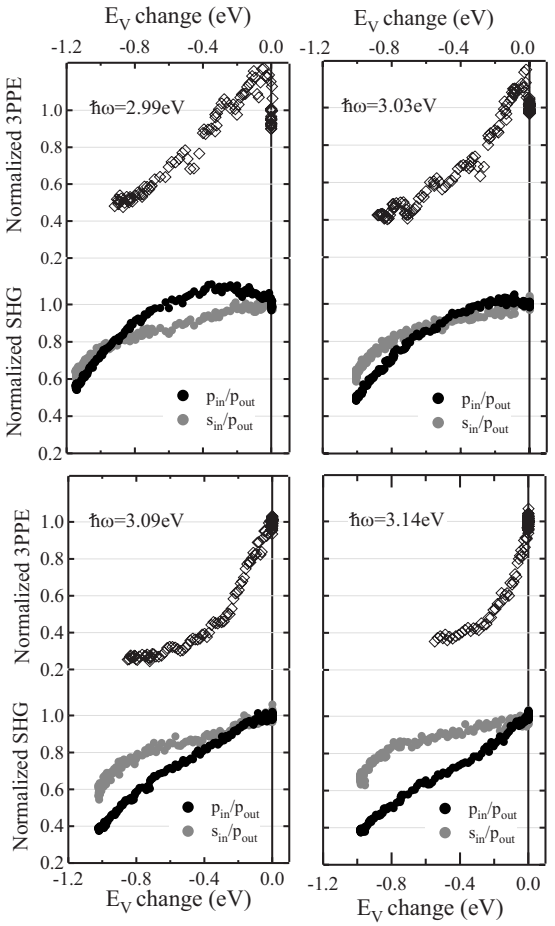

FIG. 2. Normalized total 3PPE yield in normal-emission geometry (open diamonds), normalized p_{in}-p_{out} SHG (black circles), and normalized s_{in}-p_{out} SHG (gray circles) as a function of the Cs-induced change in work function ΔE_V. The excitation energy was 2.99 eV (top left), 3.03 eV (top right), 3.09 eV (bottom left), and 3.14 eV (bottom right).

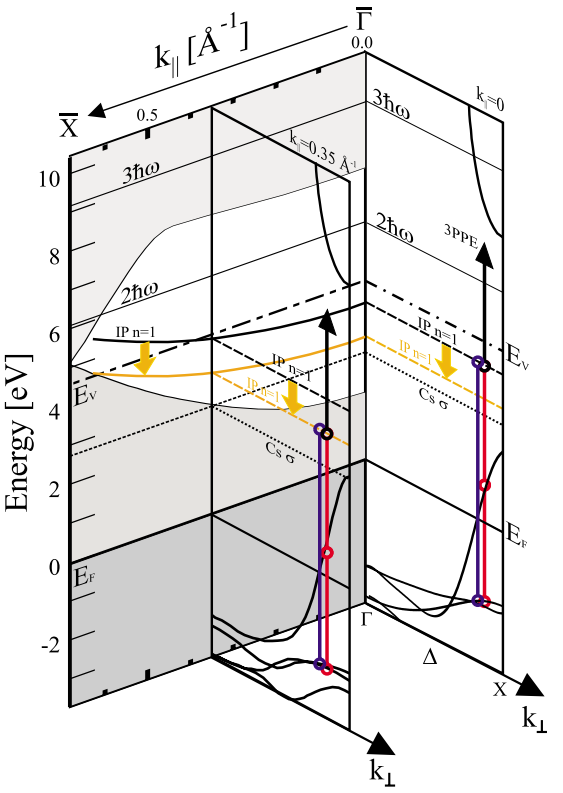

FIG. 3. (Color online) Schematic representation of a section of the surface BZ of a clean and cesiated Cu(001). Background panel: surface-projected bulk band structure (shaded area) along the $\bar{\Gamma}\bar{X}$ direction. The IP state on the clean (cesiated) surface is depicted as the solid black (orange) line. Forefront panels: Cu(001) band structure as a function of perpendicular momentum, after Burdick (Ref. 36) for $k_{\parallel}=0$ (right) and $k_{\parallel}=0.35$ Å^{-1} (center). Possible optically induced transitions at $\omega(2\omega)$ frequency are represented by the red (blue) vertical lines. 3PPE is schematically indicated by stacking a black vertical arrow on top of two 1ω transitions.

the s_{in}-p_{out} case. In Fig. 2, we report four sets of SHG measurements in the p_{in}-p_{out} and s_{in}-p_{out} geometries, performed as a function of the Cs coverage for four different excitation wavelengths. The data have been normalized to the respective clean-surface value and have been plotted as a function of the change in the work function ΔE_V with respect to the clean Cu(001), directly deduced from the low-energy cutoff of the spectra. In the top panel of each graph we reported the total 3PPE yield in normal emission normalized to its clean Cu(001) value as a function of ΔE_V.

We begin by describing the 2.99 eV data (top left panel in Fig. 2), subsequently extending the discussion to other energies. For this case, we observe that for decreasing work function the p_{in}-p_{out} measured SHG initially gradually increases, attains a very broad maximum for $\Delta E_V \approx -0.3$ eV and subsequently decreases reaching a value of 60% of the initial yield for $\Delta E_V \approx -1.1$ eV. The corresponding s_{in}-p_{out} SHG instead remains approximately constant up to $\Delta E_V \approx -0.2$ eV and then regularly drops, with constant slope, up to $\Delta E_V \approx -1.0$ eV, somehow steepening its decrease for larger ΔE_V. At the same time the integrated 3PPE signal quickly rises for small Cs coverage, exhibiting a sharp maximum for $\Delta E_V \approx -0.1$ eV, and subsequently drops with decreasing ΔE_V reaching a value of approximately 50% of the clean Cu(001) for $\Delta E_V \approx -0.9$ eV (Though SHG and photoemission were recorded simultaneously, the 3PPE vs E_V curves are typically displayed in a narrower ΔE_V range because, at large Cs exposure, the possible contribution of 2PPE electrons in the 3PPE range due to space-charge effects cannot be excluded from the data.)

With increasing excitation photon energy, the SHG and 3PPE curves undergo consistent changes. In the 3.03 eV case, the shape of the SHG and 3PPE curves strongly resemble that of the previous case but the maxima of both the p_{in}-p_{out} SHG and 3PPE are shifted toward less negative ΔE_V values; the p_{in}-p_{out} SHG peaks at $\Delta E_V \approx -0.15$ eV whereas the 3PPE maximum seems to occur just off from the $\Delta E_V = 0$ value.

In the 3.09 eV case, no maxima can be seen in any of the curves. The p_{in}-p_{out} SHG is seen around a fairly constant value for ΔE_V within −0.1 eV before starting its drop for ongoing Cs adsorption. The 3PPE curve quickly drops to 40% of its initial value before decreasing its drop rate around $\Delta E_V \approx -0.3$ eV. Finally, for 3.14 eV photon energy, the

p_{in}-p_{out} SHG exhibits a marked decrease beginning from the very early stages of Cs deposition. The 3PPE drops somehow faster than in the 3.09 eV case for small E_V change and also levels off for ΔE_V beyond roughly −0.3 eV.

In general, the s_{in}-p_{out} SHG for all the investigated photon energies does not show strong and significant variations with respect to the already described 2.99 eV case, as observable in the graphs of Fig. 2.

III. DISCUSSION

In the ED approximation, the SHG yield from a given surface depends on the Fresnel factors at the ω and 2ω frequencies and on the second-order nonlinear susceptibility tensor $\chi^{(2)}_{ijm}$. According to Ref. 19, the dependence of $\chi^{(2)}_{ijm}$ on the electronic structure of the material can be expressed as

$$\chi^{(2)}_{ijm}(2\omega) \propto \sum_{\mathbf{k},l,l',l''} M_i M_j M_m \left\{ \frac{f(E_{k,l''}) - f(E_{k,l'})}{E_{k,l''} - E_{k,l'} - \hbar\omega + i\hbar\gamma_{l'\to l''}} - \frac{f(E_{k,l'}) - f(E_{k,l})}{E_{k,l'} - E_{k,l} - \hbar\omega + i\hbar\gamma_{l\to l'}} \right\} \Big/ \left(E_{k,l''} - E_{k,l} - 2\hbar\omega + i\hbar\gamma_{l''\to l} \right). \quad (1)$$

Here, $M_i = \langle \Psi_{\mathbf{k},l} | p_i | \Psi_{\mathbf{k},l'} \rangle$ is the dipole matrix element between states $(\mathbf{k},l)$ and $(\mathbf{k},l')$ (and $M_{j(m)}$, respectively, account for the transitions between the other electronic levels involved). The electronic structure of the material enters through the eigenvalues $E_{\mathbf{k},l}$, which depend on the electron momentum $\mathbf{k}=(k_\perp,k_\parallel)$ and the band index l while $f(E)$ and $\gamma_{l\to l'}$ represent the Fermi function and the Lorentzian broadening associated with the transitions between the pertinently indexed states, respectively. Equation (1) can be further simplified by assuming the state occupation factors to be $f(E_{k,l'}) = f(E_{k,l''}) \approx 0$ and $f(E_{k,l}) = 1$, for the excited and initial states. The Cs contribution is implicitly included in Eq. (1) by admitting the adsorbate states among the energy eigenvalues $E_{\mathbf{k},l}$. For our specific case, the Cs-coverage dependence of the SHG could arise from either a change in the surface Fresnel factors or a change in $\chi^{(2)}_{ijm}$. For the Cs-coverage range under investigation, we can safely assume that no major change in the Fresnel factors takes place and accordingly proceed to model the observed SHG yield in terms of a variation in the nonlinear susceptibility $\chi^{(2)}_{ijm}$. Furthermore, the weak wavelength dependence of the Fresnel factors would not justify the wavelength-dependent variations in the SHG yields reported in Fig. 2.

We therefore discuss the electronic structure of the Cs/Cu(001) system with the aid of Fig. 3. There, a schematic representation of the system's band structure is reported, in which the electronic states at finite $k_\parallel$ are explicitly indicated. In the background panel, the surface-projected band structure of Cu along the $\bar{\Gamma}\bar{X}$ direction is reported, with the parabolically dispersing IP state drawn as the solid black line. The two panels protruding toward the forefront of the picture display the perpendicular-momentum-dependent *bulk* band structure of Cu, after Burdick,[36] for two selected values of $k_\parallel$: $k_\parallel=0$ (right) and $k_\parallel=0.35$ Å^{-1} (center), respectively. Possible electronic transitions at $\omega(2\omega)$ frequency are displayed as red (blue) lines in such panels. The possibility of observing 3PPE from two-photon-excited electronic states is schematically represented by stacking a further black vertical arrow on top of two such red lines. The correlation between SHG and 3PPE is apparent from this diagram since SHG and 3PPE involve the same set of ground, one-photon-excited and two-photon-excited electronic states, with their related transition matrix elements whereas they notably differ only in the last step. The effect of Cs adsorption will be, in first approximation, represented by the lowering of energy with respect to E_F and broadening of the IP-state (orange lines),[32] and by the appearance of the unoccupied, nondispersing, Cs σ resonance which is located, at the maximum coverage we addressed, approximately 2.6 eV above E_F (visible in the cesiated spectrum of Fig. 1).[25]

We begin our discussion by addressing the p_{in}-p_{out} SHG and the 3PPE recorded for 2.99 eV photon energy, and subsequently extend it to the other cases. Let us initially focus on the ΔE_V dependence of the integrated 3PPE data, to be discussed based on the $k_\parallel=0$ cross section of the BZ in Fig. 3. From the spectrum of Fig. 1 and the data of Ref. 30, we deduce that the near-resonant transition between d_{Cu} bands, the sp_{Cu} bands and the IP state gives by far the dominant contribution to the 3PPE. The data reported in Fig. 2 show that, as soon as E_V gets lowered by Cs adsorption, the 3PPE intensity increases, sharply peaking at around $\Delta E_V \approx -0.1$ eV. This is due to the fact that on clean Cu(001), the excitation with 2.99 eV photons does not allow the optimum two-photon resonant matching between the d_{Cu} bands and the IP state whereas this is achieved upon decreasing the IP-state energy (i.e., the work function) by Cs of the amount $\Delta E_V \approx -0.1$ eV. Choosing a value for the IP binding energy with respect to E_V at $k_\parallel=0$ of 0.59 eV,[37] and a Cu(001) work function $E_V=4.63$ eV, we deduce that the d_{Cu} bands acting as initial states in the 3PPE process are located $E_{d_{Cu}} \approx -2.04$ eV below E_F, a value in very good agreement with independent data derived from conventional photoemission experiments.[38] The decrease in 3PPE with further Cs deposition can be then assigned to the progressive detuning and broadening of the IP state from resonance occurring upon the further lowering of E_V.

The p_{in}-p_{out} SHG for 2.99 eV excitation shows two relevant differences with respect to the 3PPE. First of all, the maximum of the SHG vs E_V curve is significantly broader with respect to its 3PPE counterpart; second, it is apparently shifted to lower E_V by approximately 0.2 eV. We can account for this behavior by developing a simple model for SHG

based on the electronic structure in Fig. 3. In order to do this, we have to address the optically induced resonant electronic transitions at ω and 2ω frequency occurring throughout the BZ that go into computing $\chi^{(2)}_{ijm}$ according to Eq. (1). In this respect, the important input that we receive from the 3PPE measurements, thanks to the strong overlap between the electronic states probed by the 3PPE and the SHG, concerns the efficiency of the electronic transitions between states $(\mathbf{k},l)$, $(\mathbf{k},l')$, and $(\mathbf{k},l'')$. From Eq. (1) it can be inferred that the presence of a doubly resonant transition at specific points of the BZ yields a possibly dominant contribution to $\chi^{(2)}_{ijm}$; from the 3PPE data we have the additional information that such doubly resonant transitions can be provided by the two-photon coupling of the d_{Cu} bands with the IP state through the sp_{Cu} bands. The influence of the σ resonance on the SHG yield, which can be very strong under specific excitation conditions,[25,39,40] can be here considered negligible based on two simple arguments. First, we notice that the Cs σ resonance, according to Fig. 3, can be populated from the sp_{Cu} band only, for which the density of states is much lower with respect to the d_{Cu} bands. To this end, we notice that Cs peak in the 2PPE part of the spectrum of Fig. 1 is smaller by a factor 20 with respect to the corresponding 2PPE d_{Cu} peak. Second, the σ resonance can participate only in photoinduced transitions for which one single step is resonant while no resonance conditions can be met for the other steps. The combination of these two factors is expected to yield a much lower efficiency of this process with respect to the doubly resonant $d_{\mathrm{Cu}} \rightarrow sp_{\mathrm{Cu}} \rightarrow$ IP transition and hence a much lower SHG. We point out that, on other surfaces, like the Cu(111), resonance conditions between the sp bands and the Cs σ resonance could be more easily met for much broader Cs-coverage ranges, thereby enhancing the role of Cs in SHG at variance with our case.

Based on this observation, the model calculation of the Cs-coverage-dependent $p_{\mathrm{in}}/p_{\mathrm{out}}$ SHG yield can be performed, based on Eq. (1), under the following assumptions: (i) the dominant contribution to SHG is provided by the $d_{\mathrm{Cu}} \rightarrow sp_{\mathrm{Cu}} \rightarrow$ IP doubly resonant transition and (ii) the matrix elements involved in such transitions are considered constant as a function of both $k_{\parallel}$ and Cs coverage.[41] In this model, the calculation of $\chi^{(2)}_{ijm}$ is performed integrating all over the bulk BZ and not restricted to high-symmetry directions. The integration over $k_{\perp}$ is performed assuming that, for every $k_{\parallel}$, there exist one (or two, considering momentum directed toward or away from the surface) value of $k_{\perp}$ for which the d_{Cu} and the sp_{Cu} bands are in resonance for our excitation energy (forefront panels of Fig. 3). Then, further integration is performed all over the surface BZ under the assumption that the presence of the d_{Cu}-sp_{Cu} resonance occurs throughout the whole surface BZ with initial d_{Cu} states having a binding energy which is constant as a function of $k_{\parallel}$. With these hypotheses, the doubly resonant contributions to $\chi^{(2)}_{ijm}$ are free to occur at any location in the surface BZ where the IP-state is tued to an energy where it can contribute to the d-sp-IP double resonance.

Thus the initial-state energy $E_{k,l}$ in Eq. (1) is fixed at the energy of the d_{Cu} band region $E_{d_{\mathrm{Cu}}}$ taking part in the resonant process, the intermediate-state energy reads $E_{k,l'}=E_{d_{\mathrm{Cu}}}+\hbar\omega$ and the ($k_{\parallel}$-dependent) energy of the IP state is $E_{k,l''}$. $E_{k,l''}$ can

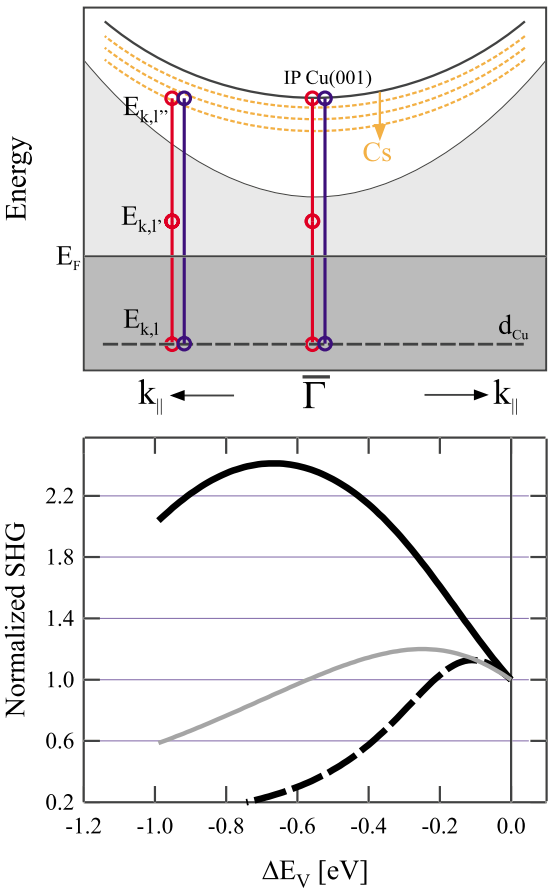

FIG. 4. (Color online) Top panel: energy diagram of the electronic states considered for the model calculation of $\chi^{(2)}_{ijm}$. The Cs-induced shift of the IP-state energy is pictorially represented. Vertical lines represent light-induced electronic transitions for different values of parallel momentum. Bottom panel: calculated dependence of $\chi^{(2)}_{ijm}$ as a function of ΔE_V performed for k-space integration over $k_{x(y)} \in [-0.5, 0.5]$ Å^{-1} (solid black line) and restricted to $\bar{\Gamma}$ (dashed black line). Here $k_{x(y)}$ are the two components of the surface parallele momentum $k_{\parallel}$. Gray line: calculated value of $\chi^{(2)}_{ijm}$ upon inclusion of a phenomenological adsorbate-induced broadening of the IP state.

in turn be written as $E_{k,l''}=\frac{\hbar^2 k_{\parallel}^2}{2m^*}+E_{\bar{\Gamma}}$, where m^* is the effective mass of the IP state and $E_{\bar{\Gamma}}$ is the Cs-coverage-dependent energy of the IP state at $\bar{\Gamma}$. We point out that since we are merely interested in finding the SHG evolution vs Cs coverage and not its absolute intensity, the value of the matrix elements between all states involved is taken as unity. The energy diagram of the states employed for calculating $\chi^{(2)}_{ijm}$ according to all the above hypothesis is shown with a one-dimensional representation in the top part of Fig. 4. Accordingly, Eq. (1) can be simplified as

$$\chi^{(2)}_{ijm} \propto \int_{k_{\parallel}} \frac{1}{i\hbar\gamma_{l\rightarrow l'}} \cdot \frac{1}{\frac{\hbar^2 k_{\parallel}^2}{2m^*} + E_{\bar{\Gamma}}(E_V) - E_{d_{\mathrm{Cu}}} - 2\hbar\omega + i\hbar\gamma_{l''\rightarrow l}}. \tag{2}$$

In the bottom part of Fig. 4 we report, as the solid black curve, a calculation of the modulus square of $\chi^{(2)}_{ijm}$ (proportional to the SHG intensity) as a function of ΔE_V performed according to our simple model, for 2.99 eV excitation energy. The theoretical curve of Fig. 4 was calculated imposing $m^*=0.94$,[30,37] keeping a fixed $\gamma_{l''\to l}=0.3$ eV (extracted from the effective width of the d bands in 2PPE, as obtained in a low-temperature Cs deposition experiment) and integrating over $k_\parallel \in [-0.5, 0.5]$ Å^{-1}, an interval more than sufficient to cover the energy range of interest for the IP state. In the same graph, the dashed curve represents the $|\chi^{(2)}_{ijm}(\Delta E_V)|^2$ dependence calculated with the same parameters as for the solid black curve but having limited the k-space integration volume to a narrow region around $\bar{\Gamma}$.

As is clearly seen in the graph, the agreement with the experimental SHG data is not satisfactory under the simple hypothesis made. The calculation of $\chi^{(2)}_{ijm}$ could however be further refined to yield a quantitatively better agreement with the data by explicitly including the adsorbate-induced broadening of the IP state.[32,42–45] Inserting a Cs-coverage-dependent broadening of $\gamma_{l''\to l}$ with a constant rate of 4.5 eV/ML, a value fully compatible with available experimental and theoretical values,[32,46] yields in fact the gray curve in the bottom panel of Fig. 4, which reproduces the experimental data significantly better. The good agreement between the experimental data and the model calculations performed under the above simple hypothesis makes us confident about the validity of our assumptions and the capability of capturing the essential physics involved in the nonlinear optical response of the material. Possible refinements involve explicitly addressing the role of single-resonant transitions in the SHG yield, although this would involve the realistic estimation of both the electric dipole matrix elements between the states involved and the phase shifts between the various SHG contributions, a task that goes beyond the scope of the present paper.

One further interesting point can be made from comparing the curves calculated with explicit integration over the whole BZ (black and gray solid curves) and the dashed curve, calculated with $\bar{\Gamma}$-limited integration. The dashed curve exhibits a ΔE_V dependence very closely resembling the one of the 3PPE signal reported in Fig. 2, peaking at $\Delta E_V \approx -0.1$ eV and quickly decreasing with decreasing E_V. This can be easily understood since the k-space region employed for calculating the dashed curve is the same as the one probed by 3PPE at normal emission. Extending the integration volume to a physically significant portion of the BZ yields a curve which is much smoother and in which the maximum of $\chi^{(2)}_{ijm}$ vs ΔE_V is clearly shifted, two features that are evident from the experimental data. The physical origin for the smoothening of the SHG features and for the ΔE_V shift with respect to 3PPE is, in our view, the variation in k-space volume contributing to the resonant SHG as a function of ΔE_V. At $\bar{\Gamma}$, in fact only one k point in the BZ will contribute to the resonant SHG whereas when resonance conditions are met at $k_\parallel \neq 0$, there will be a circle of k points in the surface BZ giving a resonant contribution to $\chi^{(2)}_{ijm}$, thereby increasing the SHG yield.

We can now briefly extend our discussion to the other polarization geometries and photon energies. Starting again with the 2.99 eV case, we begin by addressing the s_{in}-p_{out} geometry. We clearly notice that the ΔE_V dependence of the s_{in}-p_{out} SHG mainly differs from the corresponding p_{in}-p_{out} case in that the former data do not show any sign of the features that we have ascribed to the IP-state resonance in the latter curve. This can be understood based on ED selection rules, which do not allow a transition induced by s-polarized radiation between the sp_{Cu} bands and the IP state all over the BZ, due to the Δ_1-type symmetry of the states involved.[47,48] This can be also viewed as a further confirmation of the dominant role of the $n=1$ IP state in SHG for the p_{in}-p_{out} geometry.

Given the absence of a dominating double-resonant transition in the s_{in}-p_{out} geometry, the interpretation of the data cannot be reliably performed as for the p_{in}-p_{out} case. It is likely that several single-resonant transitions throughout the BZ contribute to the SHG and that the total yield is possibly also influenced by interference effects between such various contributions.[49,50] Inspecting the band structure of Fig. 3, one single-resonant process is surely represented by the d_{Cu}-sp_{Cu} coupling, that is allowed by ED selection rules for s_{in} incoming light and can occur all over the BZ. A further contribution might derive from the population of the Cs σ resonance from the sp_{Cu} bands. Given this, the regular decrease in s_{in}-p_{out} SHG can be due to the interference between a roughly coverage-independent contribution to SHG (d_{Cu}-sp_{Cu}) and a coverage-dependent one (sp_{Cu}-σ).

The spectral dependence of the p_{in}-p_{out} SHG, as diplayed in the panels of Fig. 2, can be qualitatively understood based on the same model previously outlined. In the extreme case of 3.14 eV excitation, both the 3PPE signal and the SHG exhibit a marked decrease starting from the very early stages of Cs absorption. This is because, for larger excitation energy, already for the clean Cu(001) surface the optimum resonance condition for the d_{Cu} to IP transition are met for $k_\parallel > 0$. Hence, we observe only the "decreasing" side of the resonant enhancement, due to increased broadening, that was instead observed in its entirety in the 2.99 eV case. For excitation energy between the two limiting cases of 2.99 and 3.14 eV, a gradual crossover from the former to the latter behavior is observed. We point out that the spectral dependence of the SHG is qualitatively reproduced in our calculation (not shown) while keeping all the physical parameters the same as in Fig. 4.

IV. CONCLUSION

In conclusion, we have performed a combined SHG and multiphoton photoemission study of the Cu(001) surface, with ~3 eV excitation energy, as a function of the absorption of Cs. We have modeled the SHG response of the material as dominated by a doubly resonant transition between the d_{Cu} band and the image-potential state mediated by the sp_{Cu} band. Due to the additional information directly available from 3PPE we could pinpoint the strong contribution to the total SHG yield due to electronic transitions occurring at nonzero values of parallel momentum $k_\parallel$. Our work therefore emphasizes the limits of analyzing spectroscopic SHG data without explicitly integrating over the relevant k-space vol-

ume while suggesting the possible strong influence of dephasing effects on the SHG yield when there is a strong contribution from surface states. As we have shown, the combination of nonlinear optical and photoemission measurements enhances the potential of either or both techniques as probes of the electronic structure of surfaces.

In this respect, the application of photon energies near 3 eV for performing SHG has represented a substantial advantage for this work. While these energies allowed to cover a broad enough energy range of occupied/unoccupied states of the surface, thereby increasing the information yield, at the same time it was possible to observe nonlinear photoemission using the same excitation light source. This allowed the direct matching of SHG and photoemission data. Furthermore, we point out that performing SHG with 3 eV excitation allows to access the interband excitations that cannot be reached with photons of lower energy. Our results, showing a marked decrease in the SHG yield as a function of the Cs coverage in the submonolayer regime, substantially differ with respect to SHG data gathered with lower excitation energy.[39] These latter in fact mostly probe the nonresonant free-electron response of the metal and typically exhibit an increase in the SHG signal upon alkali atom adsorption that is strictly related to the correspondent increase in the surface polarizabilty.[51] The occurrence of a resonant interband excitation pathway clearly modifies the material response with respect to what expected from a simple free-electron picture; such a modified response is highlighted in our work by the nonconventional Cs-coverage dependence of the SHG yield. It can be therefore expected that performing SHG with excitation energy near or above 3 eV and coupling it with nonlinear photoemission will prove fruitful in future nonlinear optical studies.

ACKNOWLEDGMENTS

The authors thank Wolfgang Hübner, Ulrich Höfer, and Tony Heinz for stimulating discussion. Technical assistence from F. Helbig is gratefully acknowledged. F.B. acknowledges the CNR-CNISM convention, the Università di Genova (PRA 2008) and the Fondazione Carige for financial support. H.P. acknowledges support from NSF under Grant No. CHE-0650756. W.-C.L. acknowledges support from the National Science Council of Taiwan under Grant No. 96-2112-M-003-015-MY3.

*bisio@fisica.unige.it

[1] J. Rudnick and E. A. Stern, Phys. Rev. B **4**, 4274 (1971).
[2] R. W. Boyd, *Nonlinear Optics*, 3rd ed. (Academic, San Diego, 2008).
[3] *Nonlinear Optics in Metals*, edited by K. H. Bennemann (Clarendon, Oxford, 1998).
[4] O. A. Aktsipetrov, I. M. Baranova, and Y. A. Il'inskiĭ, Sov. Phys. JETP **64**, 167 (1986).
[5] P. Guyot-Sionnest, W. Chen, and Y. R. Shen, Phys. Rev. B **33**, 8254 (1986).
[6] Y. R. Shen, Nature (London) **337**, 519 (1989).
[7] C. K. Chen, T. F. Heinz, D. Ricard, and Y. R. Shen, Phys. Rev. Lett. **46**, 1010 (1981).
[8] M. Fuyuki, K. Watanabe, D. Ino, H. Petek, and Y. Matsumoto, Phys. Rev. B **76**, 115427 (2007).
[9] H. A. Wierenga, W. de Jong, M. W. J. Prins, T. Rasing, R. Vollmer, A. Kirilyuk, H. Schwabe, and J. Kirschner, Phys. Rev. Lett. **74**, 1462 (1995).
[10] M. Nývlt, F. Bisio, J. Franta, C. L. Gao, H. Petek, and J. Kirschner, Phys. Rev. Lett. **95**, 127201 (2005).
[11] M. Fiebig, D. Fröhlich, T. Lottermoser, V. V. Pavlov, R. V. Pisarev, and H.-J. Weber, Phys. Rev. Lett. **87**, 137202 (2001).
[12] M. Nývlt, F. Bisio, and J. Kirschner, Phys. Rev. B **77**, 014435 (2008).
[13] U. Höfer, L. Li, and T. F. Heinz, Phys. Rev. B **45**, 9485 (1992).
[14] K. J. Song, D. Heskett, H. L. Dai, A. Liebsch, and E. W. Plummer, Phys. Rev. Lett. **61**, 1380 (1988).
[15] G. Lüpke, D. J. Bottomley, and H. M. van Driel, Phys. Rev. B **47**, 10389 (1993).
[16] S. Ong, X. Zhao, and K. B. Eisenthal, Chem. Phys. Lett. **191**, 327 (1992).
[17] J. Xue, C. S. Jung, and M. W. Kim, Phys. Rev. Lett. **69**, 474 (1992).
[18] M. Y. Jiang, G. Pajer, and E. Burstein, Surf. Sci. **242**, 306 (1991).
[19] T. A. Luce and K. H. Bennemann, Phys. Rev. B **58**, 15821 (1998).
[20] R. H. Williams, G. P. Srivastava, and I. T. McGovern, Rep. Prog. Phys. **43**, 1357 (1980).
[21] K. Giesen, F. Hage, H. J. Riess, W. Steinmann, R. Haight, R. Beigang, R. Dreyfus, Ph. Avouris, and F. J. Himpsel, Phys. Scr. **35**, 578 (1987).
[22] L. E. Urbach, K. L. Percival, J. M. Hicks, E. W. Plummer, and H. L. Dai, Phys. Rev. B **45**, 3769 (1992).
[23] G. Lüpke, D. J. Bottomley, and H. M. van Driel, Phys. Rev. B **49**, 17303 (1994).
[24] C. Timm and K. H. Bennemann, J. Phys.: Condens. Matter **16**, 661 (2004).
[25] S. A. Lindgren and L. Walldèn, Phys. Rev. B **45**, 6345 (1992).
[26] H. Petek, H. Nagano, and S. Ogawa, Phys. Rev. Lett. **83**, 832 (1999).
[27] V. Sametoglu, Ph.D. thesis, University of Pittsburgh, 2009.
[28] S. Ogawa and H. Petek, Surf. Sci. **363**, 313 (1996).
[29] J. Zhao, N. Pontius, A. Winkelmann, V. Sametoglu, A. Kubo, A. G. Borisov, D. Sánchez-Portal, V. M. Silkin, E. V. Chulkov, P. M. Echenique, and H. Petek, Phys. Rev. B **78**, 085419 (2008).
[30] F. Bisio, M. Nývlt, J. Franta, H. Petek, and J. Kirschner, Phys. Rev. Lett. **96**, 087601 (2006).
[31] V. Dose, W. Altmann, A. Goldmann, U. Kolac, and J. Rogozik, Phys. Rev. Lett. **52**, 1919 (1984).
[32] X. Y. Wang, R. Paiella, and R. M. Osgood, Phys. Rev. B **51**, 17035 (1995).
[33] R.-P. Pan, H. D. Wei, and Y. R. Shen, Phys. Rev. B **39**, 1229 (1989).

[34] G. Petrocelli, S. Martellucci, and R. Francini, Appl. Phys. A: Mater. Sci. Process. **56**, 263 (1993).
[35] R. Vollmer, M. Straub, and J. Kirschner, Surf. Sci. **352-354**, 684 (1996).
[36] G. A. Burdick, Phys. Rev. **129**, 138 (1963).
[37] M. Weinelt, J. Phys.: Condens. Matter **14**, R1099 (2002).
[38] J. A. Knapp, F. J. Himpsel, and D. E. Eastman, Phys. Rev. B **19**, 4952 (1979).
[39] H. Tom, C. Mate, X. Zhu, J. Crowell, Y. Shen, and G. Somorjai, Surf. Sci. **172**, 466 (1986).
[40] B. N. J. Persson and L. H. Dubois, Phys. Rev. B **39**, 8220 (1989).
[41] N. Pontius, V. Sametoglu, and H. Petek, Phys. Rev. B **72**, 115105 (2005).
[42] Ch. Reuß, I. L. Shumay, U. Thomann, M. Kutschera, M. Weinelt, Th. Fauster, and U. Höfer, Phys. Rev. Lett. **82**, 153 (1999).
[43] A. G. Borisov, A. K. Kazansky, and J. P. Gauyacq, Surf. Sci. **526**, 72 (2003).
[44] T. Fauster, M. Weinelt, and U. Höfer, Prog. Surf. Sci. **82**, 224 (2007).
[45] S. M. Dounce and H.-L. Dai, Surf. Sci. **583**, 310 (2005).
[46] A. K. Kazansky, V. M. Silkin, E. V. Chulkov, A. G. Borisov, and J.-P. Gauyacq, Phys. Rev. B **75**, 235412 (2007).
[47] J. Hermanson, Solid State Commun. **22**, 9 (1977).
[48] W. Eberhardt and F. J. Himpsel, Phys. Rev. B **21**, 5572 (1980).
[49] F. Eisert, A. P. Elg, and A. Rosén, Appl. Phys. A: Mater. Sci. Process. **60**, 209 (1995).
[50] U. Höfer, Appl. Phys. A: Mater. Sci. Process. **63**, 533 (1996).
[51] H. Ishida and A. Liebsch, Phys. Rev. B **42**, 5505 (1990).